Turbulent boundary layers on a systematically varied rough wall

Michael P. Schultz[1] and Karen A. Flack[2]
[1]*Department of Naval Architecture and Ocean Engineering, United States Naval Academy, Annapolis, Maryland 21402, USA*
[2]*Department of Mechanical Engineering, United States Naval Academy, Annapolis, Maryland 21402, USA*

(Received 18 July 2008; accepted 20 November 2008; published online 15 January 2009)

Results of an experimental investigation of the flow over a model roughness are presented. The series of roughness consists of close-packed pyramids in which both the height and the slope were systematically varied. The aim of this work was to document the mean flow and subsequently gain insight into the physical roughness scales which contribute to drag. The mean velocity profiles for all nine rough surfaces collapse with smooth-wall results when presented in velocity-defect form, supporting the use of similarity methods. The results for the six steepest surfaces indicate that the roughness function ΔU^+ scales almost entirely on the roughness height with little dependence on the slope of the pyramids. However, ΔU^+ for the three surfaces with the smallest slope does not scale satisfactorily on the roughness height, indicating that these surfaces might not be thought of as surface "roughness" in a traditional sense but instead surface "waviness."
[DOI: 10.1063/1.3059630]

I. INTRODUCTION

Surface roughness can have a significant effect on a wide range of engineering flows. Examples include, but are not limited to, industrial piping systems,[1] open channel flows,[2] turbomachines,[3] marine vehicles,[4] and aircraft.[5] Because of the ubiquitous nature of these flows in practice, there has been a long history of research on the effect of roughness on wall-bounded turbulence. Some of the earliest work was carried out by Darcy[6] who investigated the pressure losses arising from roughness in a pipe. Nikuradse[7] subsequently conducted a thorough set of experiments on the effects of uniform sand roughness on turbulent pipe flow which significantly furthered the understanding of roughness effects. Later, Moody,[8] guided largely by the findings of Colebrook,[9] developed a diagram to predict the head losses in smooth and rough pipes. The impact of the Moody diagram is difficult to overstate, as it has been a cornerstone in the field of hydraulic engineering for over 60 years.

During the same period, there has also been a large body of research focused on a better fundamental understanding of the turbulence structure over rough walls. The classical idea is that the roughness only exerts a direct influence on the turbulence within a few roughness heights of the wall, and the outer flow is unaffected except in the role the roughness plays in determining the outer velocity and length scales. This is often referred to as Townsend's hypothesis.[10] The recent review of Jiménez[11] concluded that most experimental evidence supports Townsend's hypothesis provided the roughness is not too large compared to the boundary layer thickness. Since this review, the concept of outer layer similarity in the mean velocity,[1,12–14] Reynolds stresses,[12,15–17] and large scale turbulence structure[15,18] has received further experimental support for flows over a wide range of three-dimensional roughness.

However, despite the considerable effort devoted to roughness research, many questions remain unresolved. Perhaps the most important practical issue is how to predict the frictional drag (or for internal flows, the head loss) of a generic surface based on measurements of the roughness topography. At present, it is not clear which roughness length scales and parameters best describe a surface in a hydraulic sense. Over the years, many investigators have worked on this problem (e.g., Refs. 19–28). A wide range of surface parameters have been identified as correlating with frictional drag. These include the roughness height (e.g., root mean square height k_{rms},[13] maximum peak to trough height k_t,[27] mean amplitude k_a,[28] etc.), slope,[22] density,[20] and aspect ratio.[29] Higher moments of the surface amplitude probability density function[22] as well as the first three even moments of the wavenumber power spectra of the surface amplitude[30] have also been suggested as correlating the frictional drag of rough surfaces. Even with modest success of these correlations for a specific roughness type, it can be concluded that, at present, there is no sufficiently satisfactory scaling for a generic, three-dimensional roughness. In fact, the lack of meaningful progress toward this goal led Grigson[31] to assert that the statistics of the surface profile alone could never be expected to allow reliable frictional drag predictions, and experimental tests of the surface of interest would always be required. It is hoped, however, that investigations which combine reliable fluid mechanics measurements with detailed documentation of surface topography may allow further progress on roughness scaling.

The usual avenue to studying the effect of a given parameter is to keep all other parameters fixed and examine the effect of varying the parameter of interest. This is difficult with surface roughness since for most irregular three-dimensional roughness altering the roughness height, for example, leads to concomitant changes in a host of other parameters. For this reason, there are very few data available for three-dimensional roughness in which the surface topography is systematically varied. In the present experimental

Author complimentary copy. Redistribution subject to AIP license or copyright, see http://phf.aip.org/phf/copyright.jsp

Report Documentation Page

Form Approved
OMB No. 0704-0188

Public reporting burden for the collection of information is estimated to average 1 hour per response, including the time for reviewing instructions, searching existing data sources, gathering and maintaining the data needed, and completing and reviewing the collection of information. Send comments regarding this burden estimate or any other aspect of this collection of information, including suggestions for reducing this burden, to Washington Headquarters Services, Directorate for Information Operations and Reports, 1215 Jefferson Davis Highway, Suite 1204, Arlington VA 22202-4302. Respondents should be aware that notwithstanding any other provision of law, no person shall be subject to a penalty for failing to comply with a collection of information if it does not display a currently valid OMB control number.

1. REPORT DATE	2. REPORT TYPE	3. DATES COVERED
JUL 2008		**00-00-2008 to 00-00-2008**

4. TITLE AND SUBTITLE	5a. CONTRACT NUMBER
Turbulent boundary layers on a systematically varied rough wall	5b. GRANT NUMBER
	5c. PROGRAM ELEMENT NUMBER
6. AUTHOR(S)	5d. PROJECT NUMBER
	5e. TASK NUMBER
	5f. WORK UNIT NUMBER
7. PERFORMING ORGANIZATION NAME(S) AND ADDRESS(ES) **United States Naval Academy,Department of Naval Architecture and Ocean Engineering,Annapolis,MD,21402**	8. PERFORMING ORGANIZATION REPORT NUMBER
9. SPONSORING/MONITORING AGENCY NAME(S) AND ADDRESS(ES)	10. SPONSOR/MONITOR'S ACRONYM(S)
	11. SPONSOR/MONITOR'S REPORT NUMBER(S)

12. DISTRIBUTION/AVAILABILITY STATEMENT
Approved for public release; distribution unlimited

13. SUPPLEMENTARY NOTES

14. ABSTRACT

15. SUBJECT TERMS

16. SECURITY CLASSIFICATION OF:			17. LIMITATION OF ABSTRACT	18. NUMBER OF PAGES	19a. NAME OF RESPONSIBLE PERSON
a. REPORT	b. ABSTRACT	c. THIS PAGE			
unclassified	**unclassified**	**unclassified**	**Same as Report (SAR)**	**9**	

investigation, boundary layer measurements are made of the flow over a model roughness. The series of roughness consists of close-packed pyramids in which both the height and the slope are varied. The aim of this work is to gain insight into how both roughness height and slope contribute to frictional drag for three-dimensional roughness.

II. BACKGROUND

The mean velocity in the overlap region of the inner and outer layers for smooth-wall-bounded turbulent flows is well represented by the classical log law,[32]

$$U^+ = \frac{1}{\kappa}\ln(y^+) + B, \tag{1}$$

where U^+ is the inner-normalized mean streamwise velocity, κ is the von Kármán constant ≈ 0.41, y^+ is the inner-normalized distance from the wall, and B is the smooth-wall log-law intercept ≈ 5.0. For flows over rough walls, there is an increased momentum deficit arising from the pressure drag on the roughness elements. Hama[33] noted that the primary result of this is a downward shift in the inner-normalized mean velocity profile termed the roughness function ΔU^+. The log law for flow over a rough surface is, therefore, given as

$$U^+ = \frac{1}{\kappa}\ln(y^+) + B - \Delta U^+. \tag{2}$$

Hama also observed that the mean flow in the outer layer was unaffected by the roughness and followed the same profile as the smooth wall. This is called the velocity-defect law and is given as[34]

$$\frac{U_e - U}{U_\tau} = f\left(\frac{y}{\delta}\right), \tag{3}$$

where U_e is mean streamwise velocity at the edge of the boundary layer, U_τ is the friction velocity, and δ is the boundary layer thickness.

The roughness function ΔU^+ is directly related to the increase in skin friction resulting from the roughness. For example, in a turbulent boundary layer, ΔU^+ is a function of the skin-friction coefficients C_f for the smooth and rough walls at the same displacement thickness Reynolds number Re_{δ^*} given as[33]

$$\Delta U^+ = \left(\sqrt{\frac{2}{C_f}}\right)_S - \left(\sqrt{\frac{2}{C_f}}\right)_R. \tag{4}$$

The roughness function depends on both the nature of the roughness and the Reynolds number of the flow such that

$$\Delta U^+ = f(k^+). \tag{5}$$

Once the functional dependence expressed in Eq. (5) is known for a given rough surface, the frictional drag for an arbitrary body covered with that roughness can be predicted at any Reynolds number using a computational boundary layer code[35] or a similarity law analysis.[28]

One difficulty, however, is that the roughness function is not universal among roughness types. This is clearly illustrated in Fig. 1. The results presented are for honed surfaces,[12,13] commercial steel pipe,[1] and uniform sand.[7,36] Also shown is the Colebrook-type[9] roughness function for "naturally occurring" surfaces, upon which the Moody diagram is based. The most obvious disparity in these roughness functions is their behavior in the transitionally rough regime. The critical roughness Reynolds number k^+ for both the onset of roughness effects and the approach to the fully rough behavior depends on the roughness type. A more fundamental issue that has plagued researchers is how to relate the roughness topography to k, the hydraulic roughness length scale. That is, what roughness length scale will cause collapse of the roughness functions for a range of surfaces in the fully rough flow regime? Typically the length scale which is adopted is the equivalent sand roughness height k_s, but its relation to the topography of a generic surface is unclear. k_s (Ref. 36) is defined as the size of uniform sand in Nikuradse's experiments that gives the same ΔU^+ as the surface of interest in the fully rough flow regime. This relationship can be expressed as[36]

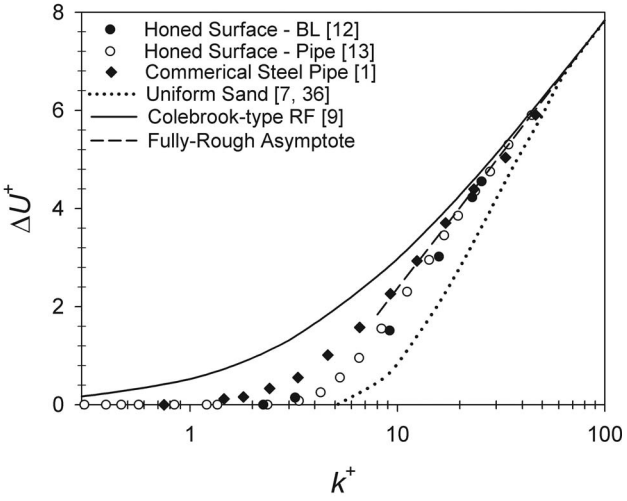

FIG. 1. Comparison of the roughness functions measured in some previous studies.

$$\Delta U^+ = \frac{1}{\kappa}\ln(k_s^+) + B - 8.5. \tag{6}$$

If, for example, one examines the surfaces in Fig. 1, k_s is simply the size of the sand grains for the uniform sand surface, while $k_s \sim 3k_{\mathrm{rms}}$ for the honed surfaces[12,13] and $k_s \sim 1.6k_{\mathrm{rms}}$ for the commercial steel pipe.[1] Clearly the roughness height alone (k_{rms} in this example) is not sufficient to specify k_s for a given surface. In the present investigation, it was hypothesized that the slope of the roughness elements should also be important in determining k_s. This is plausible since separation of the flow off of individual roughness elements should depend on the slope. Previous work by Musker[22] supports this view. The use of a model, close-packed pyramid surface allows the roughness height and slope to both be varied while other statistics such as the skewness and the kurtosis of the roughness amplitude remain fixed. In this way, it is hoped that the role of the roughness height and slope in determining k_s can be more clearly elu-

Author complimentary copy. Redistribution subject to AIP license or copyright, see http://phf.aip.org/phf/copyright.jsp

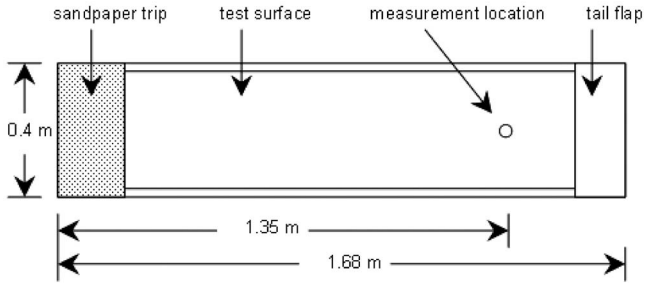

FIG. 2. Schematic of the flat plate test fixture.

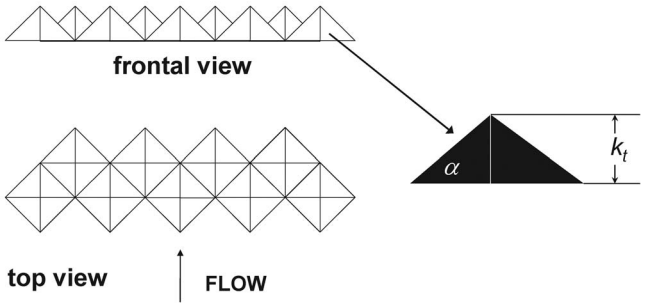

FIG. 3. Schematic of the roughness geometry and arrangement illustrating the roughness height k_t and slope angle α.

cidated. This work is part of a larger effort to collect results for three-dimensional rough surfaces in an effort to determine the roughness scales which contribute to frictional drag.

III. EXPERIMENTAL FACILITIES AND METHOD

The experiments were conducted in the high-speed water tunnel facility at the United States Naval Academy Hydromechanics Laboratory. The test section has a cross section of 40×40 cm^2 and is 1.8 m in length. A velocity range of 0–9 m/s can be produced in the test section. In the present experiments, four freestream velocities were tested ranging from 1 to 7 m/s. Flow management devices in the facility include turning vanes in the tunnel corners and a honeycomb flow straightener in the settling chamber. The honeycomb has 19 mm cells that are 150 mm in length. The area ratio between the settling chamber and the test section is 20:1. The resulting freestream turbulence intensity in the test section is $\sim$0.5%.

The test surfaces were mounted into a splitter-plate test fixture. The test fixture was installed horizontally, at mid-depth in the tunnel. The first 0.20 m of the test fixture was covered with No. 36-grit sandpaper to fix the location of transition and thicken the resulting turbulent boundary layer. A schematic of the test plate fixture is shown in Fig. 2. Further details of the experimental facility can be found in Ref. 12. All the measurements reported here were obtained at $x=1.35$ m downstream of the leading edge. Velocity profiles taken upstream of the measurement location indicated that self-similarity in velocity-defect profiles was achieved for all the test surfaces for $x\geq0.80$ m. The upper removable wall of the tunnel is adjustable to account for boundary layer growth. In the present work, this wall was set to produce a nearly zero pressure gradient boundary layer. The strength of the pressure gradient can be quantified by the acceleration parameter K given as

$$K=\frac{\nu}{U_e^2}\frac{dU_e}{dx}. \tag{7}$$

In the present experiments, $K\leq1\times10^{-8}$ in all cases, which is more than an order of magnitude below the value where pressure gradient effects are likely to influence the mean flow.[37]

The removable test specimens were fabricated from 12 mm thick cast acrylic sheet of 350 mm in width and 1.32 m in length. The rough surfaces consisted of close-packed, square, right pyramids. The four lateral edges of the pyramids were oriented at 0°, 180°, and $\pm$90° to the freestream flow (Fig. 3). Three pyramid heights k_t were tested with $k_t\approx0.30$, 0.45, and 0.60 mm. The slope angle of the lateral edges with the horizontal, α, was also varied. Slope angles of $\alpha\approx11°$, 22°, and 45° were tested. The combination of the three pyramid heights and three slope angles produced the nine rough surfaces that were tested in the present study (Fig. 4). The series of test surfaces were produced using three different custom carbide engraving cutters, one for each desired slope angle. The surfaces were machined using a CNC Haas VF-11, three-axis vertical milling machine, and ESPRIT CAD/CAM software. The machining was carried out at $\pm$45° to the direction of the flow. The tool path pitch and depth of cut were controlled to produce the desired surface texture.

In order to ensure the fidelity of the fabrication, three-dimensional topographical profiles were made of the rough surfaces using a Micro Photonics Nanavea ST300 white light chromatic aberration surface profilometer. The vertical accuracy of the system is 0.3 μm with lateral resolution of 6 μm. The data were digitized at increments of 25 μm in the lateral directions, and the sampling area was sufficient to capture a few roughness elements. An example of a surface map for the $k_t\approx0.45$ mm, $\alpha\approx11°$ roughness is presented in Fig. 5. The topographical profiles indicate that the roughness height was within $\pm$5% of the desired height for all the surfaces, while the slope angle was within $\pm$1%. The experimental test conditions along with the roughness designation used are given in Table I.

Velocity measurements were obtained using a TSI FSA3500 two-component laser Doppler velocimeter (LDV). The LDV system utilized a four beam fiber optic probe and was operated in backscatter mode. The probe included a cus-

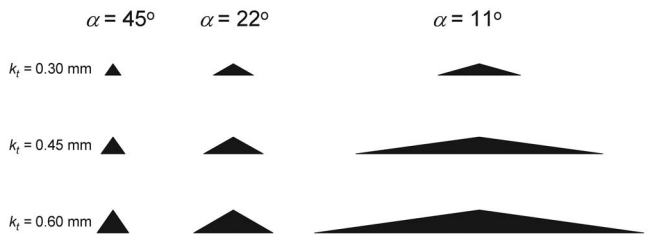

FIG. 4. Matrix of roughness test surfaces. The roughness is not drawn actual size but is to scale.

Author complimentary copy. Redistribution subject to AIP license or copyright, see http://phf.aip.org/phf/copyright.jsp

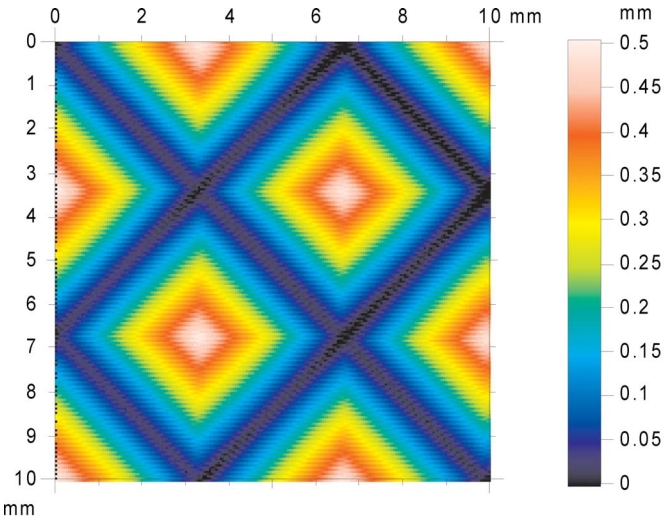

FIG. 5. (Color online) Plan view of the roughness topography for the $\alpha=22°$, $k_t=450$ μm specimen measured with a profilometer (overall uncertainty in roughness elevation: $\pm 3\times 10^{-4}$ mm).

tom beam displacer to shift one of the four beams. The result was three coplanar beams aligned parallel to the wall along with a fourth beam in the vertical plane which allowed measurements near the wall without having to tilt or rotate the probe. The system also employed 2.6:1 beam expansion optics at the exit of the probe to reduce measurement volume size. The resulting probe volume diameter d was 45 μm, with a length l of 340 μm. The measurement volume diameter, therefore, ranged from $1.9 \leq d^+ \leq 16$, while its length was $14 \leq l^+ \leq 120$ when expressed in viscous length scales. The range of d^+ values in the present experiment is similar to the smooth-wall turbulent boundary layer study of DeGraaff and Eaton.[38]

In the present investigation, 20 000 random velocity realizations were obtained at each location in the boundary layer, and the data were collected in coincidence mode. A Velmex three-axis traverse unit allowed the position of the LDV probe to be maintained to ± 5 μm in all directions. Velocity profiles consisted of approximately 42 sampling locations within the boundary layer. The flow was seeded with 3 μm diameter alumina particles. The seed volume was controlled to achieve acceptable data rates while maintaining a low burst density signal.[39]

The friction velocity was determined using two methods. The first was the total stress method.[40] This method assumes that the plateau in the total shear stress in the inner layer is equivalent to the shear stress at the wall. The total shear stress was calculated by adding the viscous and turbulent stress components. The second method employed for finding U_τ was the modified Clauser chart method.[41] Details of both methods used to find the wall shear stress can be found in Ref. 17. The normalization presented throughout the remainder of this paper uses the friction velocity obtained using the modified Clauser chart method. It should be noted that the friction velocity values found using modified Clauser chart and total stress methods agreed within $\leq 3.0\%$ for all cases tested with a mean absolute difference of 1.3%.

IV. UNCERTAINTY ESTIMATES

Estimates of the overall uncertainty in the measured quantities were made by combining their precision and bias uncertainties using the methodology specified by Moffat.[42] The 95% precision confidence limits for a given quantity were obtained by multiplying its standard error by the two-tailed t value given by Coleman and Steele.[43] Standard error estimates were determined from the variability observed in repeated velocity profiles taken on a given test surface. Bias estimates were combined with the precision uncertainties to calculate the overall uncertainties for the measured quantities. It should be noted that the LDV data were corrected for velocity bias by employing burst transit time weighting.[44] Fringe bias was considered insignificant, as the beams were shifted well above a burst frequency representative of twice the freestream velocity.[45] The resulting overall uncertainty in the mean velocity was $\pm 1.5\%$. The overall uncertainty in U_τ obtained from the modified Clauser chart method was $\pm 4\%$, while the total stress method yielded an uncertainty of $\pm 6\%$.

V. RESULTS AND DISCUSSION

The presentation of the results and discussion will be organized as follows. First, the mean flow profiles over the systematically varied roughness will be discussed in terms of both inner and outer scalings. Next, the roughness function scaling with regards to roughness height and slope will be considered.

A. Mean velocity profiles

The mean velocity profiles of the rough walls are presented using inner scaling in Fig. 6. For the sake of clarity and brevity, most of the results presented in this section are for the $k_t=450$ mm cases only, although the trends for the other roughness heights are similar. Also shown for comparison are the smooth-wall results of DeGraaff and Eaton[38] at $\mathrm{Re}_\theta=5100$. It can be seen that all of the roughness slope angles exhibit an increasing roughness function (ΔU^+) with increasing Reynolds number. One of the most striking observations is that the mean velocity profiles for the two steepest slope angles ($\alpha=22°$ and $\alpha=45°$) are nearly identical [Figs. 6(a) and 6(b)], suggesting that the slope of the present roughness elements has little influence on the resulting drag. However, the surface with the shallowest slope ($\alpha=11°$) clearly shows a smaller ΔU^+ and hence has less drag than the other surfaces. The roughness slope, therefore, can affect the drag, although slope dependence is only apparent for shallower angles. This will be discussed in greater detail in the roughness function results.

The outer-scaled mean velocity profiles are presented in velocity-defect form in Fig. 7. Again, the smooth-wall data from DeGraaff and Eaton[38] at $\mathrm{Re}_\theta=5100$ are also shown. All the mean velocity profiles exhibit agreement well within experimental uncertainty in the log law and outer regions of the boundary layer. The Clauser–Rotta[46] length scale ($\Delta=U_e^+\delta^*$) has been offered as an alternative outer length scale for the mean velocity profile. It has the advantage of being based on an integral length parameter (δ^*) rather than δ,

Author complimentary copy. Redistribution subject to AIP license or copyright, see http://phf.aip.org/phf/copyright.jsp

TABLE I. Experimental test conditions.

Designation	k_t (μm)	α (°)	U_e (m s^{-1})	Re_θ	ε (μm)	U_τ Clauser chart (m s^{-1})	U_τ Total stress (m s^{-1})	δ (mm)	δ^+	k_t^+	ΔU^+
45_300_1	300	45	1.01	3 430	200	0.0432	0.0432	28.1	1 180	12.6	1.7
45_300_3	300	45	3.01	11 450	80	0.137	0.138	30.3	3 960	39.2	6.2
45_300_5	300	45	4.99	20 850	10	0.231	0.233	33.3	7 340	66.1	7.8
45_300_7	300	45	7.01	30 610	70	0.328	0.328	34.1	10 850	95.5	9.1
45_450_1	450	45	1.01	3 510	280	0.0458	0.0455	28.5	1 250	19.8	3.3
45_450_3	450	45	3.01	11 570	60	0.142	0.145	29.9	4 130	62.2	7.0
45_450_5	450	45	5.00	20 060	150	0.240	0.242	31.2	7 140	103.0	8.8
45_450_7	450	45	7.01	28 580	200	0.339	0.334	31.7	10 220	145.2	9.8
45_600_1	600	45	1.00	3 960	220	0.0498	0.0496	30.1	1 470	29.3	5.4
45_600_3	600	45	3.01	12 320	50	0.159	0.159	31.0	4 740	91.7	9.3
45_600_5	600	45	5.00	21 760	150	0.254	0.253	32.2	7 930	147.7	10.3
45_600_7	600	45	7.01	30 100	200	0.354	0.355	31.8	10 920	206.0	10.9
22_300_1	300	22	1.01	3 430	200	0.0448	0.0447	28.6	1 240	13.0	2.6
22_300_3	300	22	3.01	11 280	100	0.138	0.135	30.2	4 020	39.9	6.4
22_300_5	300	22	5.01	21 020	170	0.234	0.227	32.2	7 300	68.0	8.3
22_300_7	300	22	7.02	28 610	180	0.326	0.318	31.6	9 990	94.9	9.0
22_450_1	450	22	1.01	3 460	200	0.0467	0.0461	27.3	1 240	20.4	3.5
22_450_3	450	22	3.01	10 400	40	0.146	0.149	28.0	3 900	62.7	7.0
22_450_5	450	22	5.00	17 730	10	0.246	0.248	29.0	6 850	106.4	8.3
22_450_7	450	22	7.01	25 510	130	0.346	0.342	29.2	9 800	151.5	9.5
22_600_1	600	22	1.01	3 770	240	0.0493	0.0493	28.7	1 370	28.7	5.1
22_600_3	600	22	3.00	11 450	250	0.155	0.151	29.4	4 290	87.5	8.7
22_600_5	600	22	5.00	19 780	260	0.257	0.250	30.6	7 500	147.1	9.9
22_600_7	600	22	7.00	28 030	300	0.363	0.357	30.5	10 740	211.3	10.8
11_300_1	300	11	1.01	3 070	100	0.0429	0.0423	26.3	1 090	12.5	1.1
11_300_3	300	11	3.00	9 180	70	0.127	0.127	26.2	3 140	35.9	3.8
11_300_5	300	11	5.00	15 820	60	0.214	0.215	26.9	5 490	61.2	5.3
11_300_7	300	11	7.02	21 590	100	0.303	0.298	26.5	7 800	88.2	6.1
11_450_1	450	11	1.00	2 910	130	0.0435	0.0445	25.8	1 080	18.8	1.5
11_450_3	450	11	3.01	8 640	120	0.127	0.129	25.2	3 030	54.2	3.9
11_450_5	450	11	5.01	14 870	270	0.217	0.221	26.5	5 450	92.8	5.3
11_450_7	450	11	7.02	19 980	320	0.307	0.305	25.2	7 440	132.7	6.2
11_600_1	600	11	1.00	3 480	340	0.0429	0.0439	28.3	1 180	25.0	2.2
11_600_3	600	11	3.00	10 710	400	0.125	0.126	29.5	3 550	72.1	4.2
11_600_5	600	11	5.01	18 620	400	0.208	0.207	31.2	6 290	120.9	5.2
11_600_7	600	11	7.01	25 670	480	0.296	0.288	31.0	8 940	173.0	6.2

whose definition is somewhat arbitrary. It also can account for Reynolds number dependence through U_e^+. The outer-scaled mean velocity profiles are presented in velocity-defect form using the Clauser–Rotta scaling in Fig. 8. The results show excellent collapse throughout the log law and outer regions of the boundary layer for both the smooth and rough walls. These mean flow results support Townsend's hypothesis[10] that the surface condition has no direct effect on the outer flow but simply plays a role in setting the outer length and velocity scales. This is in agreement with earlier work by the authors[12,14] for range of three-dimensional roughness of various heights and types. Recent results[47] show that this mean flow similarity is very robust and is maintained for flows over three-dimensional roughness in which the roughness height is a significant fraction of the boundary layer thickness (relative roughness as large as $k_t/\delta \approx 0.2$). Collapse of mean flow profiles for rough and smooth walls in velocity-defect form is important in accurate prediction of drag, since mean flow similarity in outer variables is assumed both when relating laboratory results to full scale using boundary layer similarity laws[48] as well as when using wall function models for numerical computations.[35]

B. Roughness function ΔU^+

The roughness function results for the two steepest roughness slope angles ($\alpha=22°$ and $\alpha=45°$) are shown in Fig. 9 along with the results for Nikuradse's[7,36] uniform sand. For the present results, the roughness height k was initially taken to be the peak-to-trough height k_t. Figure 9 shows reasonable agreement between the roughness functions observed on the $\alpha=22°$ and $\alpha=45°$ surfaces. Any dif-

Author complimentary copy. Redistribution subject to AIP license or copyright, see http://phf.aip.org/phf/copyright.jsp

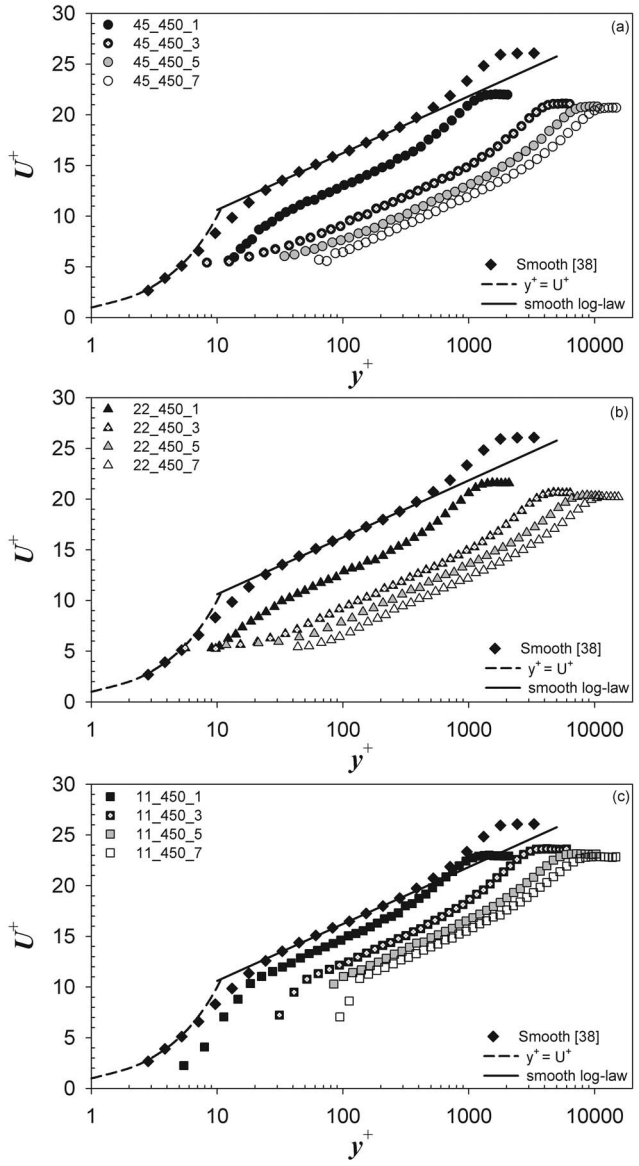

FIG. 6. Mean velocity profiles in inner variables (overall uncertainty in U^+: ±4%).

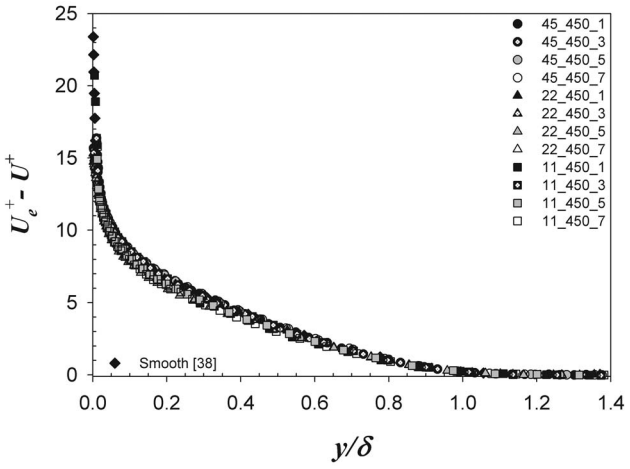

FIG. 7. Mean velocity profiles in outer variables using classical scaling (overall uncertainty in $U_e^+ - U^+$: ±5%)

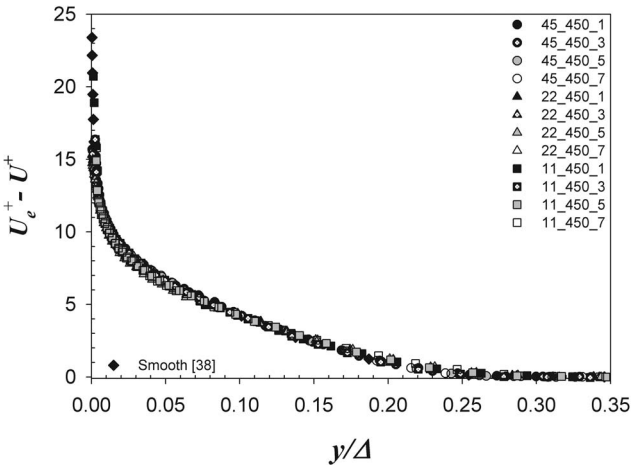

FIG. 8. Mean velocity profiles in outer variables using the Clauser–Rotta length scale (overall uncertainty in $U_e^+ - U^+$: ±5%).

ferences that are observed do not indicate any clear influence of the slope angle. It appears, therefore, if the roughness slope is steep enough, the roughness function scales entirely on k, and the roughness slope is irrelevant. These roughness slope angles combined with the sharp edges of the present roughness most likely cause total flow separation in the lee of the individual roughness elements regardless if the slope angle is 22° or 45°, leading to large form drag.

The results at the higher Reynolds numbers were used to evaluate the equivalent sand roughness height k_s using Eq. (6). For the $\alpha=22°$ and $\alpha=45°$ surfaces, this gives $k_s \approx 1.5k_t$. The results for the steeper roughness slopes are plotted in Fig. 10 using this scaling. It can be seen that the roughness function for these surfaces displays a similar inflectional behavior in the transitionally rough regime as the uniform sand. However, it appears that for the present roughness, the inflectional behavior is even more pronounced than

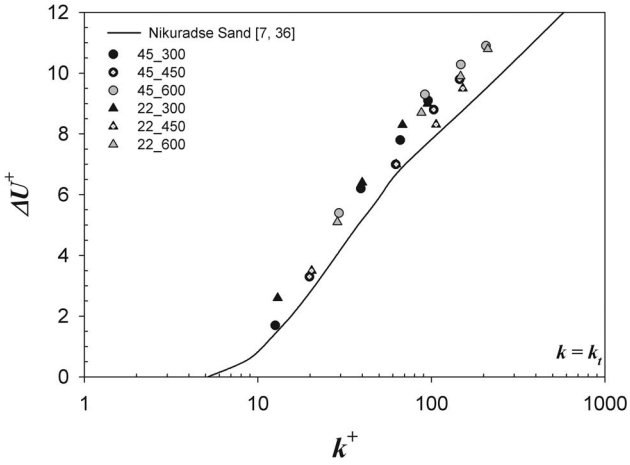

FIG. 9. Roughness function results for the $\alpha=22°$ and $\alpha=45°$ specimens using $k=k_t$ (overall uncertainty in ΔU^+: ±10%).

Author complimentary copy. Redistribution subject to AIP license or copyright, see http://phf.aip.org/phf/copyright.jsp

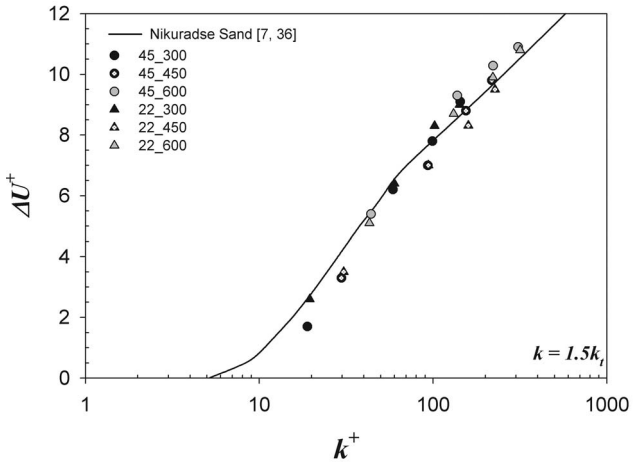

FIG. 10. Roughness function results for the $\alpha=22°$ and $\alpha=45°$ specimens using $k=1.5k_t$ (overall uncertainty in $\Delta U^+: \pm 10\%$).

is observed for the uniform sand. More low roughness Reynolds number data would be useful to confirm this observation.

The roughness function results for the shallowest roughness slope angle ($\alpha=11°$) are shown in Fig. 11 along with the data for uniform sand of Nikuradse.[7,36] Note that for the present results, the roughness height k was taken to be the peak-to-trough height k_t. The results clearly indicate that the roughness function for the $\alpha=11°$ surfaces does not scale on k. For example, examination of the higher Reynolds number results reveals that doubling the roughness height has little, if any, effect on ΔU^+. This seems to indicate that the separation in the lee of the shallow slope roughness is not complete as is the case of the steeper slopes. That is not to say that there is no separation behind the elements. Both the behavior of the roughness function and the sharp-edged nature of the roughness elements would point to at least mild separation. The fact that there is a positive ΔU^+ for these surfaces indicates that their skin friction is above smooth-wall values and there is some form drag on the roughness elements. Attempts were made to use alternative length scales to collapse the

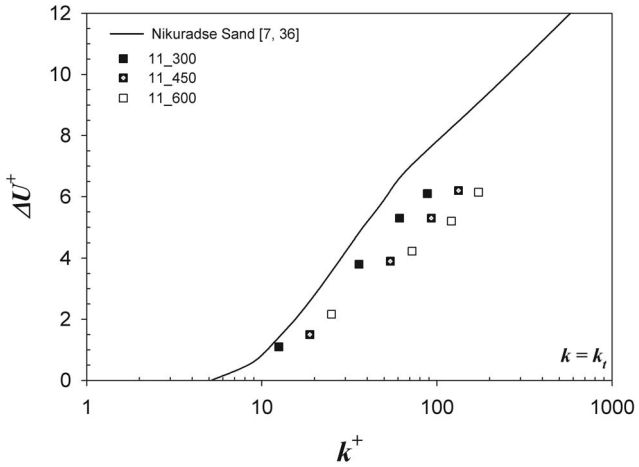

FIG. 11. Roughness function results for the $\alpha=11°$ specimens using $k=k_t$ (overall uncertainty in $\Delta U^+: \pm 10\%$).

roughness function for these surfaces. This met with little success because of the geometric similarity of the surfaces. If, for example, the roughness wavelength is used, the result is effectively the same as using k, since the wavelength of the roughness varies in the same fashion as the roughness height since the slope of the surfaces is the same.

Rough surfaces in which the roughness function does not scale on k have been reported on extensively in the literature (e.g., Refs. 41 and 49–51). However, most, if not all of this work, has focused on the flow over two-dimensional roughness, specifically, transverse bars in which the spacing between bars is nearly the same as the bar height. Perry *et al.*[52] first showed that this type of roughness displayed an anomalous roughness function scaling and termed it "*d*-type" roughness. This is in contrast to most roughness types in which ΔU^+ scales in some fashion on k, commonly called k-type roughness. In the case of two-dimensional bars, the reason for the anomalous roughness function scaling stems from the fact that the flow skims over the cavity between the bars leading to the formation of stable vortical flow cells between elements. To the authors' knowledge the inability of the roughness function to scale on the roughness height has not been previously documented in the literature for any type of three-dimensional roughness. The mechanism for the lack of k scaling in the present three-dimensional roughness is obviously much different than for the case of two-dimensional bars. For the present roughness, there appears to be a critical slope below which the roughness no longer behaves like "roughness" in a traditional sense but instead acts as surface "waviness."

Nakato *et al.*[53] noted analogous behavior for two-dimensional sinusoidal wave roughness. They observed that the roughness function behaved like that for uniform sand provided the slope was greater than ~6°. In cases where the slope was <6°, the roughness function did not follow the uniform sand roughness function, and they referred to these surfaces as "wavy" walls. They did not note any lack of scaling on k for these surfaces. However, this may have been simply because they did not systematically vary k in the experiments while holding the slope fixed. This is an important point because, unlike Nikuradse's exhaustive study in which both the Reynolds number and roughness height were varied, many studies only vary the Reynolds number while holding the roughness height fixed. If one examines the results presented in Fig. 11 for any single roughness height, it would likely be concluded that the roughness function does scale on k since an increase in the roughness Reynolds number leads to an increasing roughness function. However, when the results are taken in their entirety, it is obvious this is not the case. There may, therefore, be more surfaces that have been identified as k-type based on results from a single roughness height that are not.

The present results, taken in light of the recent study of Napoli *et al.*,[54] do provide some physical insight into this behavior. Napoli *et al.* carried out a numerical investigation of the flow over irregularly distributed two-dimensional roughness. The wall consisted of corrugated roughness constructed by the superposition of sinusoids of random ampli-

Author complimentary copy. Redistribution subject to AIP license or copyright, see http://phf.aip.org/phf/copyright.jsp

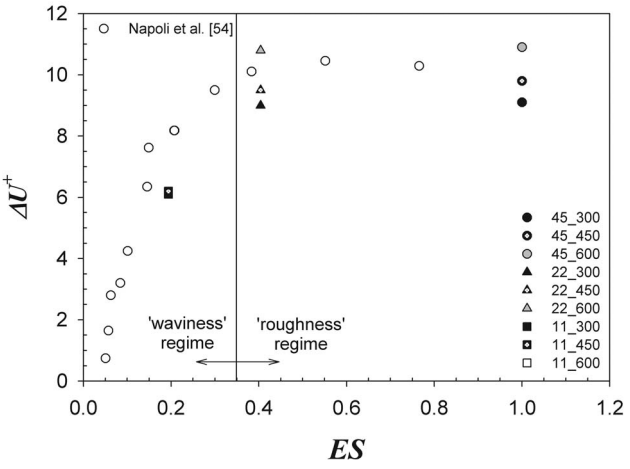

FIG. 12. Roughness function vs ES (overall uncertainty in ΔU^+: ±10%).

tude. In this work, they developed a roughness parameter termed the effective slope (ES), defined as follows:

$$\mathrm{ES} = \frac{1}{L}\int_L \left|\frac{\partial r}{\partial x}\right| dx, \tag{8}$$

where L is the sampling length, r the roughness amplitude, and x the streamwise direction. In their study, roughness with effective slopes in the range of $0.042 \leq \mathrm{ES} \leq 0.760$ were tested, and it was concluded that the roughness function is strongly dependent on ES. Specially, they concluded that ΔU^+ scales linearly on ES for $\mathrm{ES} \leq 0.15$. For larger values of ES, ΔU^+ scales on ES in a nonlinear fashion, reaching a maximum at $\mathrm{ES} \sim 0.55$ and declining slightly for $\mathrm{ES} > 0.55$. It should be noted that all of their test cases were carried out at the same friction Reynolds number. The change in the scaling which they contend occurs at $\mathrm{ES} \sim 0.15$ corresponds roughly to the point where frictional and form drag on the roughness elements are equal.

In the present work, the range of effective slopes tested was $0.19 \leq \mathrm{ES} \leq 1.0$. The results of Napoli *et al.*[54] are presented in Fig. 12 along with the present results from the highest Reynolds number cases. The trends observed in the results are similar. The present results show that for the steepest roughness cases ($\mathrm{ES} = 0.40$ or 1.0), the roughness function does not scale on ES. The variation in ΔU^+ observed is due to differences in k, and the roughness function scales entirely on the roughness Reynolds number [Eq. (5)]. This corresponds to the roughness flow regime in which form drag on the roughness elements is much larger than the frictional drag. For the smallest slope tested ($\mathrm{ES} = 0.19$), ΔU^+ is reduced compared to higher ES cases and ΔU^+ does not scale on k. This corresponds to the waviness flow regime in which ES is an important parameter in scaling the roughness function. In this regime, the frictional drag is non-negligible. Based on the present results and those of Napoli *et al.*,[54] it is proposed that a regime transition occurs at $\mathrm{ES} \sim 0.35$. For $\mathrm{ES} > \sim 0.35$ (the roughness flow regime), the roughness function is independent of the effective slope and scales entirely on the roughness Reynolds number. For $\mathrm{ES} < \sim 0.35$ (the roughness flow regime), the roughness function is strongly dependent on the effective slope, while the roughness height has little influence. In light of the results of Napoli *et al.*,[54] this transition appears to correspond physically to the slope at which pressure drag on the roughness elements overwhelms the frictional drag. However, a detailed survey of the flow structure very near the roughness elements is needed to better understand the flow physics which give rise to the transition from the roughness to the waviness regime.

VI. CONCLUSION

Results of an experimental investigation of the flow over a model roughness in which both the height and the slope were systematically varied have been presented. The mean velocity profiles for all the rough surfaces collapse with smooth-wall results when presented in velocity-defect form. The slope of the roughness appears to be an important parameter in the prediction of drag for roughness with shallow angles; however, its importance diminishes with increasing slope until the point where the roughness height is the dominant scaling parameter. The results for the steepest surfaces indicate that the roughness function ΔU^+ scales almost entirely on the roughness height with little dependence on the slope of the pyramids. However, ΔU^+ for the three surfaces with the smallest slope does not scale satisfactorily on the roughness height, indicating that these surfaces might not be thought of as surface roughness in a traditional sense but instead surface waviness. There appears to be a critical effective slope, ($\mathrm{ES} \sim 0.35$) that delineates the flow regimes.

ACKNOWLEDGMENTS

The authors would like to thank the Office of Naval Research, Contract No. N00014-05-WR-2-0231, for financial support of this research. Many thanks also go to Mr. Mike Superczynski for machining the test specimens and Mr. Don Bunker of the USNA Hydromechanics Laboratory staff for providing technical support. The authors are also grateful for the many helpful comments of the referees, which significantly strengthened the final manuscript.

[1] L. I. Langelandsvik, G. J. Kunkel, and A. J. Smits, "Flow in a commercial steel pipe," J. Fluid Mech. **595**, 323 (2008).
[2] M. F. Tachie, D. J. Bergstrom, and R. Balachandar, "Roughness effects on the mixing properties in open channel turbulent boundary layers," J. Fluids Eng. **126**, 1025 (2004).
[3] J. P. Bons, R. P. Taylor, S. T. McClain, and R. B. Rivir, "The many faces of turbine surface roughness," J. Turbomach. **123**, 739 (2001).
[4] M. P. Schultz, "Effects of coating roughness and biofouling on ship resistance and powering," Biofouling **23**, 331 (2007).
[5] A. K. Kundu, S. Ragunathan, and R. K. Cooper, "Effect of aircraft surface smoothness requirements on cost," Aeronaut. J. **104**, 415 (2000).
[6] H. Darcy, *Recherches Experimentales Relatives au Mouvement de L'Eau dans les Tuyaux* (Mallet-Bachelier, Paris, 1857).
[7] J. Nikuradse, 1933, "Laws of flow in rough pipes," NACA Technical Memorandum 1292.
[8] L. F. Moody, "Friction factors for pipe flow," Trans. ASME **66**, 671 (1944).
[9] C. F. Colebrook, "Turbulent flow in pipes with particular reference to the transition between smooth and rough pipe laws," J. Inst. Civ. Eng. **11**, 133 (1939).
[10] A. A. Townsend, *The Structure of Turbulent Shear Flow*, 2nd ed. (Cambridge University Press, Cambridge, 1976).

Author complimentary copy. Redistribution subject to AIP license or copyright, see http://phf.aip.org/phf/copyright.jsp

[11] J. Jiménez, "Turbulent flows over rough walls," Annu. Rev. Fluid Mech. **36**, 173 (2004).
[12] M. P. Schultz and K. A. Flack, "The rough-wall turbulent boundary layer from the hydraulically smooth to the fully rough regime," J. Fluid Mech. **580**, 381 (2007).
[13] M. A. Shockling, J. J. Allen, and A. J. Smits, "Roughness effects in turbulent pipe flow," J. Fluid Mech. **564**, 267 (2006).
[14] J. S. Connelly, M. P. Schultz, and K. A. Flack, "Velocity-defect scaling for turbulent boundary layers with a range of relative roughness," Exp. Fluids **40**, 188 (2006).
[15] Y. Wu and K. T. Christensen, "Outer-layer similarity in the presence of a practical rough-wall topography," Phys. Fluids **19**, 085108 (2007).
[16] K. A. Flack, M. P. Schultz, and T. A. Shapiro, "Experimental support for Townsend's Reynolds number similarity hypothesis on rough walls," Phys. Fluids **17**, 035102 (2005).
[17] K. A. Flack, M. P. Schultz, and J. S. Connelly, "Examination of a critical roughness height for outer layer similarity," Phys. Fluids **19**, 095104 (2007).
[18] R. J. Volino, M. P. Schultz, and K. A. Flack, "Turbulence structure in rough- and smooth-wall boundary layers," J. Fluid Mech. **592**, 263 (2007).
[19] D. Bettermann, "Contribtion a l'etude de la couche limite turbulent le long de plaques regueuses," Center National de la Recherche Scientifique Report No. 65–6, 1965.
[20] F. A. Dvorak, "Calculation of turbulent boundary layers on rough surfaces in pressure gradients," AIAA J. **7**, 1752 (1969).
[21] R. B. Dirling, "A method for computing rough wall heat transfer rates on re-entry nosetips," AIAA Pap. 73-763 (1973).
[22] A. J. Musker, "Universal roughness functions for naturally-occurring surfaces," Trans. Can. Soc. Mech. Eng. **1**, 1 (1980).
[23] J. S. Medhurst, "The systematic measurement and correlation of the frictional resistance and topography of ship Hull coatings, with particular reference to ablative antifoulings," Ph.D. thesis, University of Newcastle-upon-Tyne, 1989.
[24] D. R. Waigh and R. J. Kind, "Improved aerodynamic characterization of regular three-dimensional roughness," AIAA J. **36**, 1117 (1998).
[25] J. A. van Rij, B. J. Belnap, and P. M. Ligrani, "Analysis and experiments on three-dimensional, irregular surface roughness," J. Fluids Eng. **124**, 671 (2002).
[26] J. P. Bons, "*St* and c_f augmentation for real turbine roughness with elevated freestream turbulence," J. Fluids Eng. **124**, 632 (2002).
[27] M. P. Schultz and K. A. Flack, "Turbulent boundary layers over surfaces smoothed by sanding," J. Fluids Eng. **125**, 863 (2003).
[28] M. P. Schultz, "Frictional resistance of antifouling coating systems," J. Fluids Eng. **126**, 1039 (2004).
[29] P. R. Bandyopadhyay and R. D. Watson, "Structure of rough-wall boundary layers," Phys. Fluids **31**, 1877 (1988).
[30] R. L. Townsin and S. K. Dey, "The correlation of roughness drag with surface characteristics," Proceedings of the RINA International Workshop on Marine Roughness and Drag, London, UK, 1990 (Wiley, New York, 1938).
[31] C. W. B. Grigson, "Drag losses of new ships caused by Hull finish," J. Ship Res. **36**, 182 (1992).
[32] C. M. Millikan, 1938, "A critical discussion of turbulent flows in channels and circular tubes," Proceedings of the Fifth International Congress on Applied Mechanics, Cambridge, MA (Royal Institute of Naval Architects, London, 1990), pp. 386–392.
[33] F. R. Hama, "Boundary-layer characteristics for rough and smooth surfaces," Soc. Nav. Archit. Mar. Eng., Trans.tea **62**, 333 (1954).
[34] T. von Kármán, "Mechanishe aehnlichkeit and turbulenz," Nachr. Ges. Wiss. Goettingen, Math.-Phys. Kl., pp. 58−76 (1930).
[35] V. C. Patel, "Perspective: Flow at high Reynolds number and over rough surfaces—Achilles Heel of CFD," J. Fluids Eng. **120**, 434 (1998).
[36] H. Schlichting, *Boundary-Layer Theory*, 7th ed. (McGraw-Hill, New York, 1979).
[37] V. C. Patel, "Calibration of the Preston tube and limitations on its use in pressure gradients," J. Fluid Mech. **23**, 185 (1965).
[38] D. B. DeGraaff and J. K. Eaton, "Reynolds-number scaling of the flat-plate turbulent boundary layer," J. Fluid Mech. **422**, 319 (2000).
[39] R. J. Adrian, in *Fluid Mechanics Measurements*, edited by R. J. Goldstein (Hemisphere, Washington, DC, 1983).
[40] P. M. Ligrani and R. J. Moffat, "Structure of transitionally rough and fully rough turbulent boundary layers," J. Fluid Mech. **162**, 69 (1986).
[41] A. E. Perry and J. D. Li, "Experimental support for the attached-eddy hypothesis in zero-pressure gradient turbulent boundary layers," J. Fluid Mech. **218**, 405 (1990).
[42] R. J. Moffat, "Describing the uncertainties in experimental results," Exp. Therm. Fluid Sci. **1**, 3 (1988).
[43] H. W. Coleman and W. G. Steele, "Engineering application of experimental uncertainty analysis," AIAA J. **33**, 1888 (1995).
[44] P. Buchhave, W. K. George, and J. L. Lumley, "The measurement of turbulence with the laser-Doppler anemometer," Annu. Rev. Fluid Mech. **11**, 443 (1979).
[45] R. V. Edwards, "Report of the special panel on statistical particle bias problems in laser anemometry," ASME J. Fluids Eng. **109**, 89 (1987).
[46] F. H. Clauser, "Turbulent boundary layers in adverse pressure gradients," J. Aeronaut. Sci. **21**, 91 (1954).
[47] I. P. Castro, "Rough-wall boundary layers: Mean flow universality," J. Fluid Mech. **585**, 469 (2007).
[48] P. S. Granville, "The frictional resistance and turbulent boundary layer of rough surfaces," J. Ship Res. **1**, 52 (1958).
[49] S. Leonardi, P. Orlandi, and R. A. Antonia, "Properties of *d*- and *k*-type roughness in turbulent channel flow," Phys. Fluids **19**, 125101 (2007).
[50] D. H. Wood and R. A. Antonia, "Measurements in a turbulent boundary layer over *d*-type surface roughness," J. Appl. Mech. **42**, 591 (1975).
[51] L. Djenidi, R. Elavarasan, and R. A. Antonia, "The turbulent boundary layer over transverse square bars," J. Fluid Mech. **395**, 271 (1999).
[52] A. E. Perry, W. H. Schofield, and P. N. Joubert, "Rough wall turbulent boundary layers," J. Fluid Mech. **37**, 383 (1969).
[53] M. Nakato, H. Onogi, Y. Himeno, I. Tanaka, and T. Suzuki, 1985, "Resistance due to surface roughness," Proceedings of the 15th Symposium on Naval Hydrodynamics, pp. 553–568.
[54] E. Napoli, V. Armenio, and M. DeMarchis, "The effect of the slope of irregularly distributed roughness elements on turbulent wall-bounded flows," J. Fluid Mech. **613**, 385 (2008).

Author complimentary copy. Redistribution subject to AIP license or copyright, see http://phf.aip.org/phf/copyright.jsp